

CFD Simulations of Crosswind Impinging on a High Speed Train Model

A. Bouferrouk¹, D. Hargreaves² and H. Morvan²

¹College of Engineering, Mathematics and Physical Sciences, University of Exeter, Exeter, UK

²Faculty of Engineering, University of Nottingham, Nottingham, UK

Abstract

This paper presents a methodology and results for CFD simulations of a simplified high speed train configuration in a strong crosswind, at different yaw angles, in static and moving ground cases. The simulations are transient and the time-averaged forces and rolling moment around the train increase with yaw angle in a range typical of that seen with real trains. Velocity and streamline plots have produced flow features commonly observed around high speed trains, particularly the existence of a large scale vortex shed from the train nose and its subsequent breakdown at large yaw angles. In addition, CFD data suggests that the pressure distribution around the train is almost independent of the position along its length. The methodology for aerodynamic simulation in this study forms part of ongoing efforts to design automated wind alarm systems for UK high speed trains, to mitigate the effects of strong crosswinds.

Introduction

The UK government have recently given the go ahead for plans to replace and expand its high speed rolling stock through the Super Express and HS2 programs. For modern lightweight, flexible high speed trains aerodynamic loads due to strong crosswinds can cause overturning, passenger discomfort, increased fuel consumption, increased hazard of falling trees, enhanced slip-streams and increased risk of power loss due to swaying motions of catenary and pantographs [1]. UK high speed trains do not have wind alarm systems to warn against strong crosswinds, unlike in Germany where operational systems are installed on rail tracks. Trains in the UK are stopped when the crosswind speed reaches 80mph. This causes service delays with increased passenger frustration and economic loss to train operators. A feasibility study was proposed to UK's national operator Network Rail to design an automated early wind alarm system that predicts the risk of train overturning in crosswinds. This way, trains would for instance slow down rather than stop. The alarm system requires information on time-averaged aerodynamic coefficients, wind characteristics, train dynamics, and if applicable, rail structures like embankments, viaducts, bridges, and tunnel exits. The idea of an early wind alarm system was investigated in [2] for a road vehicle, while Delaunay et al. [3] described an automated system for the TGV Méditerranée in France. Experimental and numerical results were reported for a high-sided lorry in [2] but no CFD work was presented for trains. This study was commissioned to devise a CFD methodology to simulate crosswinds on trains to derive mean aerodynamic force and moment coefficients using the capabilities of commercial software. In experiments, obtained data can only be described over a limited range but CFD offers the possibility to investigate the crosswind behaviour over a wider range of conditions.

Numerical Set-up and boundary conditions

A CAD model for the UK's high speed Pendolino train could not be released by the manufacturers and it was not possible to build any realistic 3D models based on the drawings supplied by

Network Rail. Real trains are often not used for aerodynamic studies owing to their geometrical complexities; instead, simplified models are used. An idealised train configuration was first used by Chiu and Squire [4] in their experimental work on crosswind effects on high speed trains. Despite being a simple configuration compared to real trains, the model replicates many of the flow features observed around real trains, and so it was adopted for this study. The idealised train has a profile defined by

$$|y|^n + |z|^n = c^n \quad (1)$$

There are two main parts: the main body and a nose, both described by equation (1). The train body has a cylindrical shape of height $D = 125$ mm. For the train body, the value of constant c is 62.5mm and $n = 5$. For the nose, the cross-section follows a semi-elliptical profile with a major diameter of $1.28D$ and n reduces uniformly from $n = 5$ to $n = 2$ at the nose tip. The slenderness of the model is 10. The idealised train model is shown in figure 1 as created in ANSYS GAMBIT. This idealised train model approximates the leading car of a high speed train that receives, in practice, the highest aerodynamic loading under crosswinds [1]. Some workers used multiple cars to simulate more realistic flow conditions and allow the boundary layer to develop behind the leading car. But for crosswinds, the following cars are only slightly affected. For ease of computation the bogie, suspensions, track and rails are not simulated. The train is considered a solid, rigid body with no internal air flow.

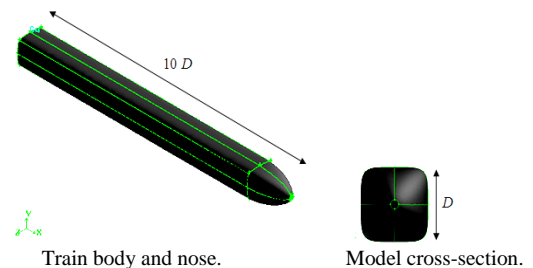


Figure 1: The idealised train model configuration [4].

The meshing was created by considering key flow physics and the required level of accuracy to represent the geometry. Boundary layers were grown from the main surfaces of the train and size functions were used to grow the mesh away using geometric progression series rules as in [5]. The aim was to create as much as possible of the computational domain using structured grid for minimum computational errors; a structured mesh was applied to the rectangular train body. Non-conformal interfaces were used to link the structured and unstructured meshes. The details of the mesh are shown in figure 2. All computations, using ANSYS CFX 11.0 which is based on the finite volume method, were performed with a single mesh, created in GAMBIT 2.4.6, of about 4 million cells. The model was placed inside a cylinder (or a turntable). This mesh is referred to as the inner mesh. The solid train model is subtracted from the cylindrical volume resulting in a train-shaped blockage.

The outer mesh, or the fetch, consists of the surrounding flow domain which has a rectangular shape. The cylindrical turntable is then subtracted from the fetch. A non-conformal grid interface links the two volume meshes. With this method the fetch can rotate relative to the train model and turntable by the required angle, avoiding the need to create a new mesh for each wind direction. The turntable and fetch are shown in figure 3.

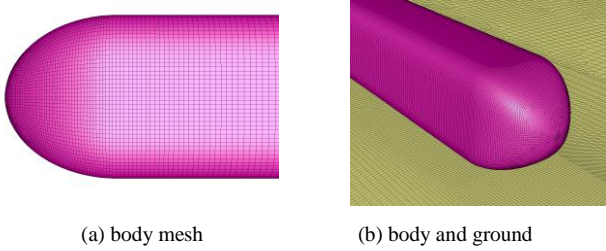


Figure 2: Close up of the mesh around the idealised train.

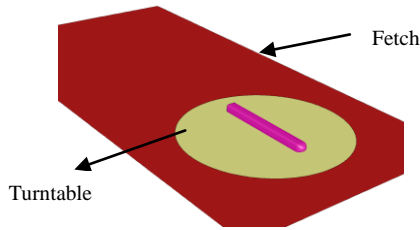


Figure 3: Fetch and turntable.

This technique is also used in wind tunnel testing to allow rotation of the test vehicle towards different wind directions [5]. It is worth noting, however, that this is only valid for a flat terrain and may not be suitable for cases where embankments or viaducts are simulated. A sufficiently large distance from the inlet boundary to the train's front was used to ensure that the velocity and pressure fields are uniform at the inlet and to allow the flow to develop by the time it reached the train. The domain also extends behind the body to ensure that the outflow condition does not affect the near-body wake. Moreover, the model is sufficiently far from the side walls to minimise near wall effects. The origin of the coordinate system is located in the track plane exactly at the level of the track. The x -axis is parallel to the train's direction of motion, the y -axis is the lateral, side force direction, and the vertical z -axis is the direction along which the lift force is applied. When a crosswind of speed V_w impinges on a train of speed V_v , the yaw angle θ , the prevailing wind angle α , and the resultant relative wind vector V_r are as shown in figure 4.

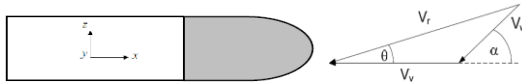


Figure 4: The coordinate system, train and wind velocities.

To simulate a moving train, it is possible to consider the train static and move the ground with a velocity equal to $-V_v$. In the CFD model, the velocity of the train is thus $(0,0,0)$ and the ground velocity is $(-V_v, 0, 0)$. While simulating a moving ground in experiments is difficult, CFD provides the ability to model the motion of the train with respect to the ground with a crosswind. For the static case, the boundary condition at the inlet reduces to uniform velocity profile equal to the mean crosswind and with the wind and yaw angles being equal. However, when the train moves, simulation of atmospheric boundary layer (ABL) is required. Robinson and Baker [6] showed that inclusion of an ABL for a transport vehicle is necessary for producing accurate flow physics. In particular, the train motion induces a skewed oncoming crosswind velocity profile. With the ABL, the resultant crosswind varies with height z above the ground, i.e. $V_w = V_w(z)$

$$V_w(z) = \frac{u^*}{\kappa} \ln\left(\frac{z+z_0}{z_0}\right), \quad u^* = \kappa V_{ref} / \ln\left(\frac{z_{ref}+z_0}{z_0}\right) \quad (2)$$

Here, u^* is the friction velocity, $\kappa=0.4$ is the Von Karman's constant, the reference velocity V_{ref} is measured at the reference height $z_{ref} = 6$ m, and the ground roughness is $z_0 = 0.01$ m for open country terrain. In the implementation of the wind alarm system, V_{ref} would be the wind speed measured at the nearest weather station at a railway line. The (inlet) resultant wind velocity vector as seen by the train driver is $\mathbf{u} = (-V_w \cos(\alpha) - V_v, (V_w \sin(\alpha), 0)$. At the reference height, one can show that [2] the yaw angle and resultant relative wind may be expressed as

$$\theta = \cot^{-1}\left[\left(\frac{V_v}{V_w} + \cos\alpha\right) \frac{1}{\sin\alpha}\right], \quad V_r = \sqrt{V_w^2 + V_v^2 - 2V_w V_v \cos(\pi - \alpha)} \quad (3)$$

In the CFD method, user-defined functions were implemented to customise the inlet flow conditions which change with each yaw angle. The airflow past the train is assumed stationary, incompressible, isothermal and turbulent in the whole flow domain. No-slip boundary conditions were used on the train surface and the ground floor. Symmetry boundary conditions were used on the fetch side walls and on its ceiling. Similar to realistic trains, the distance of $0.15D$ between the ground and train was included. The inlet conditions for the turbulent kinetic energy, k , and dissipation rate, ε may be defined as in [7]

$$k_{inlet} = u_*^2 C_\mu^{-0.5}, \quad \varepsilon(z) = \frac{u_*^3}{\kappa(z+z_0)} \quad (4)$$

where C_μ is a turbulence constant. The parameters k_{inlet} and $\varepsilon(z)$ provide the basic time and length scales of the modelled turbulence. The SST turbulence model was used for all computations. The ground was represented as a smooth, moving plane with no modelled roughness. The downstream section was set as a pressure boundary (outlet). Because of the complexity of the flow being simulated, it was not possible to solve the flow using a steady state solution. Thus, all runs were performed in a transient mode, i.e. using unsteady RANS with a constant time step of 0.05s, which was considered small enough to resolve the fluctuations in the aerodynamic forces. Though this is less accurate than LES or DES, the prime interest is in the averaged forces so the use of unsteady RANS is reasonable. A similar approach was used in [2, 5] on a high-sided truck which gave CFD data comparable to experimental results. All computations were performed on a high performance server (Prandtl) which houses 12 computing nodes, each node having 2 CPUs, and each CPU is dual core with 1GB RAM each. The simulations were run in parallel using the Grid Partition tool in the parallel server. The computations used 4 partitions to balance the speed of calculations with minimising communication at grid interfaces.

Results and discussions

The convergence of the CFD computations is based on monitoring, in time, the residuals as well as the forces. Convergence is achieved when both the side and lift forces deviate less than 0.001% in conjunction with residuals that are nearly fully converged. For a yaw angle of 30° , the convergence of lift and side forces for a static case is shown in figure 5 while that for a moving ground case is shown in figure 6. From Figures 5 and 6, one can observe that with the moving ground simulation, the force histories exhibit small periodic oscillations compared with the static case. The absence of periodic oscillations in convergence studies is only possible with perfectly smooth models. The time-averaged forces are estimated using a time period excluding the initial transients; the averaging time was generally larger for the moving ground case.

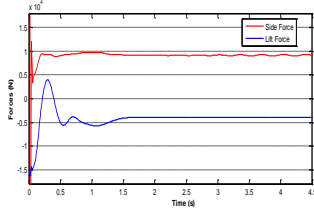


Figure 5: Time histories of side and lift forces (static ground).

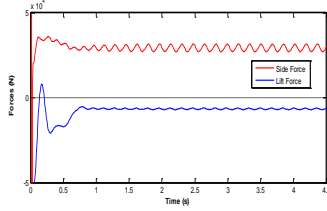


Figure 6: Time histories of side and lift forces (moving ground).

The mean side, lift and moment coefficients are expressed as

$$C_S = \frac{F_S}{0.5\rho A_{ref} V_W^2}, C_L = \frac{F_L}{0.5\rho A_{ref} V_W^2}, C_{MR} = \frac{M_R}{0.5\rho A_{ref} V_W^2 h_L} \quad (5)$$

where F_S , and F_L are the time-averaged side, and lift forces respectively. M_R is the time-averaged rolling moment about the x axis and $h_L = 2.875$ m is the (full scale) moment arm and equals the height from the track level to the top of the train. The full scale train's length is $L = 25$ m. The parameters $\rho = 1.225$ kg.m⁻³, $A_{ref} = 61.64$ m² are respectively the air density and the (reference) side area. These coefficients only depend on the actual shape of the train, not on its size or speed. For a static case, simulations were run with a strong crosswind of 80 mph at seven yaw angles from 0° to 90°, in step of 15°. The results, including the drag force, are shown in figure 7.

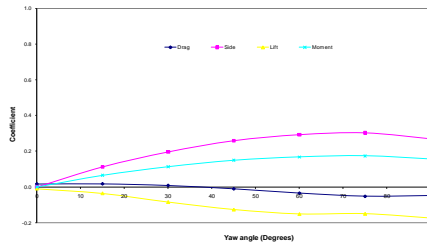


Figure 7: Mean force and moment coefficients (static ground).

The lift coefficient decreases with yaw angle. This is associated with flow acceleration underneath the train which causes a larger area of low pressure compared with the top of the train, resulting in a down force. At a zero yaw angle, the side force coefficient is zero. Then, it increases steadily with yaw angle till about 75° before it starts to decrease. This side force behaviour with yaw angle is consistent with other investigations on high speed trains; for instance the study in [4]. The decrease in side force at very high yaw angles is believed to be the consequence of vortex breakdown occurring at this range. The results also indicate that the side force is the major contributor in crosswinds in accordance with other findings e.g. [1]. The rolling moment coefficient varies in a similar fashion to the side force as expected, since the rolling moment is the result of both the lift and side forces but with the side force being the main contributor. For side-wind stability, the roll moment is responsible for wheel unloading. The drag coefficient, important only for energy considerations and not safety, decreases with increasing the yaw angle and actually becomes positive at yaw angles beyond 35°. A similar behaviour was observed in [2] though in reality the total drag including the wake does not decrease.

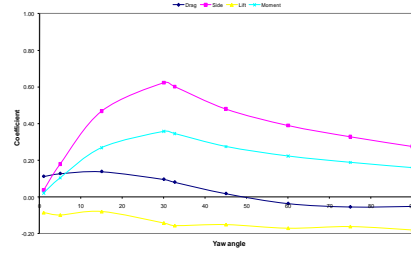


Figure 8: Mean force and moment coefficients (moving ground).

For the moving ground case, figure 8, the side and rolling moment coefficients increase with yaw angle up to $\theta = 30^\circ$ after which further increase in θ leads to a reduction in these coefficients, almost linearly. Compared with the static case, the forces and rolling moment are higher due to the contribution from a moving vehicle. Figure 9 shows time-averaged velocity vector plots at different locations L/D along the train cross section at $\theta = 30^\circ$ ($L/D = 0$ is at the middle of the train's surface).

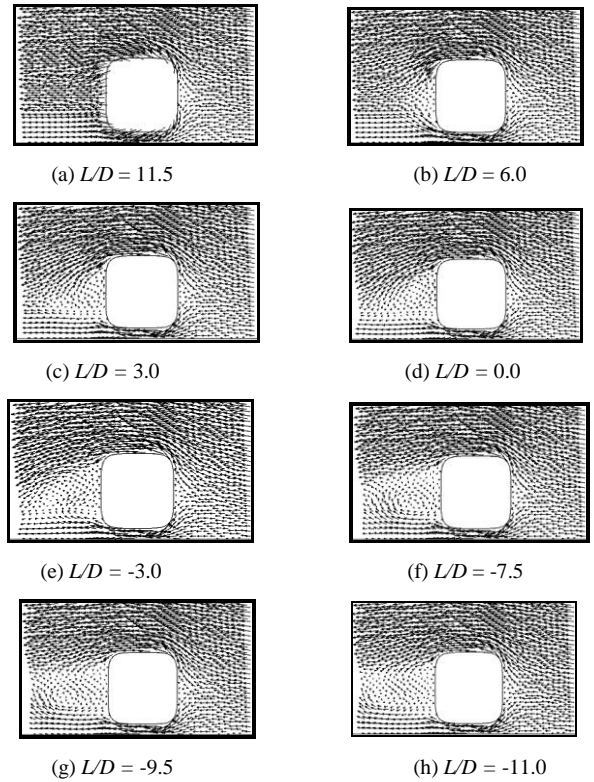


Figure 9: Velocity vectors along the train's cross section at $\theta = 30^\circ$.

As can be seen from figure 9, there is a large separation region on the downstream side of the train (leeward side), extending over much of its surface starting from aft of the nose ($L/D = 11.5$) till the back end of the train ($L/D = -11.5$) and towards the wake. This is presumably linked to the strong inclined vortex forming around the nose region which is then shed along the surface. At $L/D = 0$ (train centre), the recirculation region caused by the vortex flow is adjacent to the walls of the train, as seen in figure 9 (d). Then, it slowly drifts away from the surface as the flow develops further towards the wake. One also notices the flow acceleration in two distinct regions: the train's top surface and the gap between the ground and the train's bottom surface. On the windward side, there is a large stagnation region at the nose where the crosswind impinges on the train body, followed by a region of relatively mild pressure over most of the remaining surface. Both the underside of the train and its top surface are regions of low pressure, in accordance with figure 9. On the leeward side, negative pressure exists everywhere due to the

existence of a relatively strong rotating vortex. The existence of the lower pressure region on the leeward side of the train can explain the increased side force and roll moment. For low to high yaw angles, we investigated how the flow develops around the train, with attention to flow development on the downward side. Investigation of the mean streamlines at different yaw angles, figure 10, shows that while at $\theta = 1^\circ$ the flow is almost parallel to the train's lateral wall the flow on the downward side slowly develops into a region dominated by a large separation zone at large values of θ . This vortex structure is the consequence of the strong interactions between the flow deflected by the nose, the flow accelerating from the train's roof, and the flow emanating from underneath the train. The observed flow physics at large yaw angles occurring on the leeward side is characteristic of cross wind flows seen in wind tunnel flow visualisations [8].

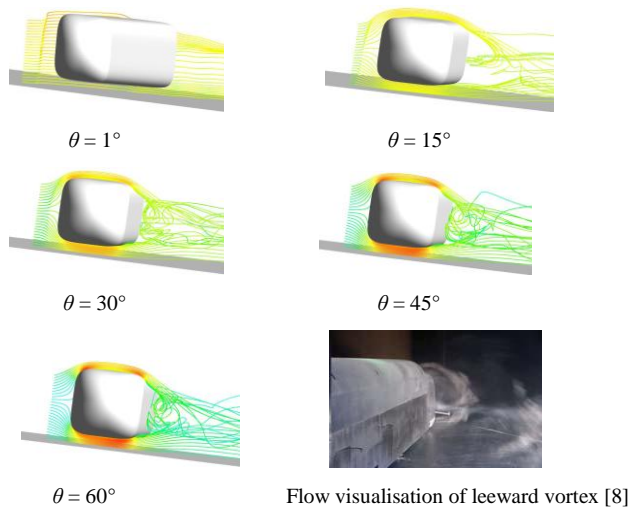


Figure 10: Mean streamlines at different yaw angles.

The mean pressure coefficient, C_p , is plotted in figure 11 around the circumference of the train at different locations along its length at $\theta = 60^\circ$, for the static case.

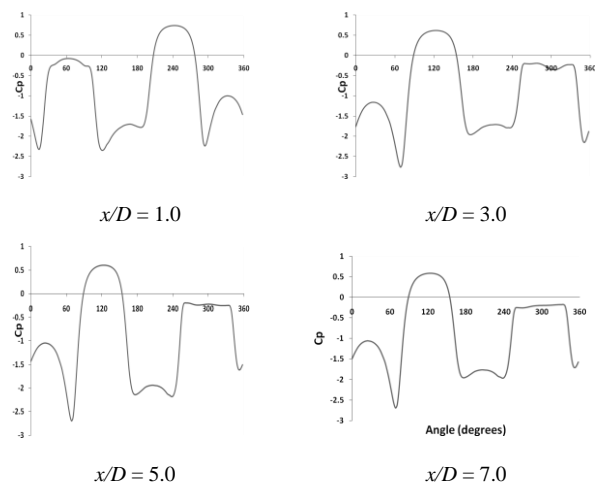


Figure 11: Mean C_p distribution around the train's surface, static case.

From figure 11 it is seen that the pressure distribution does not change much along the train except in a small region close to the nose ($x/D \leq 1.0$). Since the 60° yaw angle flow is characterised by a strong shedding vortex on the leeward side, the pressure distribution implies that the separated vortex is statistically homogeneous in the axial direction. Similar observations were reported in the experimental works of Robinson & Baker [6] who

showed that the pressure distribution around a high speed train at very high yaw angles is almost independent of the axial position. The moving ground creates more negative pressure and thus more lift as seen in figure 12 for a yaw angle of 75° .

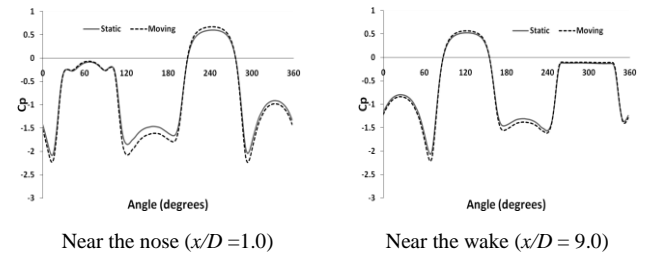


Figure 12: Mean C_p distribution at $\theta = 70^\circ$, moving and static cases.

Conclusions

This study has presented a methodology for CFD simulation of a simplified train configuration when it runs under a steady crosswind in static and moving ground scenarios. The approach is explained in terms of the meshing strategy using the turntable concept and the careful modelling of ABL with a moving ground. Despite the geometry being far simpler than real trains and the CFD methodology not fully tested, the results obtained were quantitatively and qualitatively consistent with previous research. Aerodynamic data from this work can be used in a dynamics study to investigate how forces and moments time histories may affect the dynamics of a train. The CFD methodology has been successful with an idealised geometry, but in the future more realistic configurations based on existing high speed trains should be simulated. Other dangerous scenarios like embankments, and tunnel exits should be investigated. For such cases the turntable approach may not be suitable. Various crosswind gusts should be looked at in addition to using advanced modelling like LES.

Acknowledgments

The study was financially supported by Network Rail, UK.

References

- [1] Diedrichs, B., On Computational Fluid Dynamics Modelling of Crosswind Effects for High-speed Rolling Stock, *Proc. Instn Mech. Engrs*, 217 Part F: J. Rail and Rapid Transit, 2003.
- [2] Stirling, M., Quinn, A.D., Hargreaves, D.M., Cheli, F., Sabbioni, E., Tomassini, G., Delaunay, D., Baker, C.J., Morvan, H., A Comparison of Different Methods to Evaluate the Wind Induced Forces on a High Sided Lorry, *Wind. Eng. Industrial Aerodynamic*, 98, 2010, 10-20.
- [3] Delaunay, D., Cléon, L. M, Sacré, C., Sourget, F., and Gautier, P. E, Designing a Wind Alarm System for the TGV-Méditerranée. 11th International Conference on Wind Engineering., Texas, USA, 2003.
- [4] Chiu, T., Squire, L., An Experimental Study of the Flow over a Train in a Crosswind at Large Yaw Angles up to 90° , *Wind. Eng. Industrial Aerodynamic*, 45, 1992, 47-74.
- [5] Hargreaves, D.M., Morvan, H.P., Initial Validation of Cross Wind Effects on a Static High-Sided Vehicle, *NAFEMS International Journal of CFD Case Studies*, 2008.
- [6] Robinson, C.G., Baker, C.J., The Effect of Atmospheric Turbulence on Trains, *Wind. Eng. Industrial Aerodynamic*, 34, 1990, 251-272.
- [7] Richards, P.J. & Hoxey, R., Appropriate Boundary Conditions for Computational Wind Engineering Models using the $k-\epsilon$ Model, *Wind. Eng. Industrial Aerodynamics*, 46 & 47, 1993, 145-153.
- [8] Orellano, A., Schober, M., Aerodynamic Performance of a Typical High Speed Train, Proceedings of the 4th WSEAS Conference on Fluid Mechanics and Aerodynamics, Greece, 2006.